Wiener-Khinchin Theorem in a Reverberation Chamber

Qian Xu, Lei Xing, Yongjiu Zhao, Zhihao Tian, *Student Member*, *IEEE*, and Yi Huang, *Senior Member, IEEE*

***Abstract*—The use of Wiener-Khinchin theorem in the reverberation chamber reveals the relationships between a number of important parameters: the coherence bandwidth and the *Q* factor measured in the time domain, the coherence time and the *Q* factor measured in the frequency domain, the *K*-factor and the Doppler spectrum as well as the *K*-factor and the total scattering cross section (TSCS). The lower bound of the average *K*-factor is also given. Different physical quantities which share similar mathematical insights are unified. Analytical derivations are given and results are validated by measurements.**

***Index Terms*— Wiener-Khinchin theorem, reverberation chamber, *Q* factor, *K*-factor, Doppler shift, total scattering cross section, absorption cross section.**

I. Introduction

Reverberation chambers (RCs) have been used in the electromagnetic compatibility area for many years. Recently, the applications of RC have been extended to communication channel emulations [1-7]. Due to the statistical mechanism and the system level measurement ability, RCs can be used in fifth generation (5G) communication system measurements [1-7]. Existing applications including bit error rate (BER) measurement [1], total radiated power (TRP) measurements [5], total isotropic sensitivity (TIS) measurements [6], antenna diversity gain measurements [7], and antenna efficiency measurements [8, 9].

Coherence is an important concept in channel emulation. In an RC, the relationship between the coherence bandwidth (Δf) of the measured *S*-parameters and the *Q* factor of the RC has been experimentally investigated [10-13], efforts have been made to obtain analytical and empirical equations between Δf and *Q* [10-13]. By applying the Wiener-Khinchin theorem to the frequency domain response (S_{21}) of the RC, the relationship between the coherence bandwidth and the chamber decay time (τ_{RC}) has been given in [14].

In this paper, based on the contribution in [14], we generalize the application of Wiener-Khinchin theorem from frequency domain in [14] to the time domain and space domain. We show that not only in the frequency domain, but also in the time domain and the space domain (the moving of a stirrer), the Wiener-Khinchin theorem can be used and the relationship between different physical quantities (coherence bandwidth, *Q* factor, coherence time, *K*-factor, Doppler spectrum, total scattering cross section and absorption cross section) can be revealed. The use of the Wiener-Khinchin theorem in this paper unifies different physical quantities in an RC, and the relationship between them can be well understood and quantified.

The Wiener-Khinchin theorem is briefly reviewed in Section II, followed by its applications and derivations in the frequency domain, time domain and space domain. In Section III, measurements are conducted to verify the results. Discussion and conclusions are summarized in Section IV.

II. Theory and Applications

The well-known Wiener-Khinchin theorem (also known as the Wiener–Khinchin–Einstein theorem or the Khinchin–Kolmogorov theorem) gives the relationship between the autocorrelation function and the power spectrum. Suppose $S(f)$ is a complex function, the autocorrelation function $R(\partial f)$ is defined as

$$R(\partial f) \equiv \int_{-\infty}^{\infty} S(f)S^*(f+\partial f)df \tag{1}$$

where * means complex conjugate, and the inverse Fourier transform (IFT) of $S(f)$ is $s(t)$

$$s(t) = \mathcal{F}^{-1}[S(f)] = \int_{-\infty}^{\infty} S(f)e^{j2\pi ft}df \tag{2}$$

Wiener-Khinchin theorem tells us that [15]

$$R(\partial f) = \mathcal{F}[|s(t)|^2] = \int_{-\infty}^{\infty} |s(t)|^2 e^{-j2\pi\partial ft}dt \tag{3}$$

where $\mathcal{F}[|s(t)|^2]$ is actually the power spectrum. For the measurements in this paper, the functions are defined over a finite region and the values outside the defined regions can be set as zero. Thus, (1) - (3) do not have infinite integral boundaries for data processing and Wiener-Khinchin theorem

Manuscript received **.

This work was supported in part by the National Natural Science Foundation of China (61701224 and 61601219) and Nature Science Foundation of Jiangsu Province (BK20160804).

Q. Xu, L. Xing, Y. Zhao are with College of Electronic and Information Engineering, Nanjing University of Aeronautics and Astronautics, Nanjing 211106, China (e-mail: emxu@foxmail.com).

Z. Tian is with the College of Optoelectronic Science and Engineering, National University of Defense Technology, Changsha 410073, China.

Y. Huang is with the Department of Electrical Engineering and Electronics, The University of Liverpool, Liverpool L69 3GJ, UK. (e-mail: yi.huang@liv.ac.uk).

is valid as long as the Fourier transform of functions in (1) – (3) exist. Since Δf has been used to represent the coherence bandwidth or average mode bandwidth in this paper, we do not use Δf but use ∂f instead as the variable in (1) and (3).

In an RC, a typical measurement setup is shown in Fig. 1, Ant 1 and Ant 2 are connected to the port 1 and port 2 of a vector network analyzer (VNA), respectively. A computer controls the rotation of the stirrer and records the measured *S*-parameters from the VNA at different stirrer positions. Because Wiener-Khinchin theorem is a mathematical conclusion, the function $S(f)$ in (1) can be treated as a transfer function depends on the frequency, it can also be replaced by a time domain response depends on time $s(t)$ or a transfer function depends on the position of the stirrer $S(\theta)$. These three cases are analyzed as follows, and we use $\langle\cdot\rangle_m$, $\langle\cdot\rangle_a$ and $\langle\cdot\rangle_f$ to represent the averaging process caused by rotating mechanical stirrers (mechanical stir), moving antennas (source stir) and frequency averaging (frequency stir) respectively.

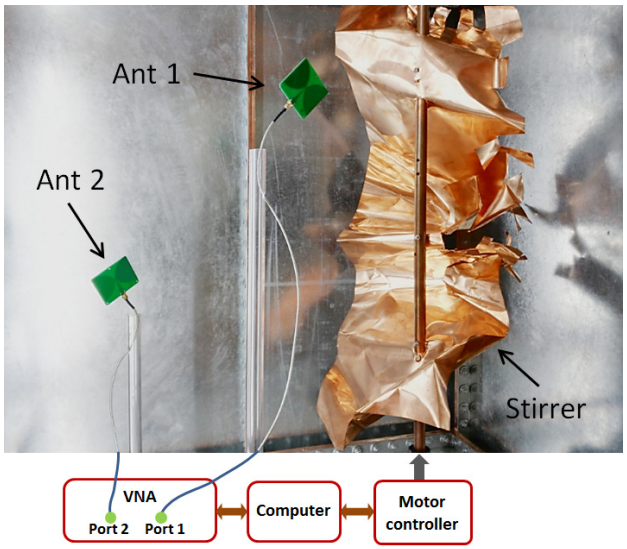

Fig. 1. RC measurement setup at Nanjing University of Aeronautics and Astronautics (NUAA), the dimensions are 1.2 m (L) × 1.2 m (H) × 0.8 m (W), the lowest usable frequency is about 1 GHz.

A. Frequency Domain

Suppose $S(f)$ in (1) is the measured S_{21} for different stirrer positions in an RC and f is the frequency, $s(t) = \mathcal{F}^{-1}[S(f)]$ is the IFT of $S(f)$. $s(t)$ is actually the time domain response of the RC, the square of it is the power delay profile (PDP), which decays exponentially with time [14]:

$$\mathrm{PDP}(t) = \langle|s(t)|^2\rangle_m = P_0 e^{-t/\tau_{RC}}, \quad t > 0 \tag{4}$$

where $\langle\cdot\rangle_m$ means the assemble average over different stirrer positions, τ_{RC} is the chamber decay time. From (3), it can be found that [14]

$$\langle R(\partial f)\rangle_m = \mathcal{F}[\langle|s(t)|^2\rangle_m] = \mathcal{F}\left[P_0 e^{-t/\tau_{RC}}\right] \tag{5}$$

thus the average autocorrelation [14]

$$\langle R(\partial f)\rangle_m = \frac{P_0 \tau_{RC}}{1 + j2\pi\tau_{RC}\partial f} \tag{6}$$

The use of Wiener-Khinchin theorem in the frequency domain clarifies the relationship between the coherence bandwidth and τ_{RC} [14]. If the magnitude of (6) is normalized to its peak value, it has been given in [14] that

$$|\langle R(\partial f)\rangle_m|_{norm} = \frac{1}{\sqrt{1 + (2\pi\tau_{RC}\partial f)^2}} \tag{7}$$

and τ_{RC} can be related to the Q factor of the RC measured in the time domain [16]:

$$Q_{TD} = \omega\tau_{RC} = \frac{Q_{FD}}{\eta_{1tot}\eta_{2tot}} = \frac{16\pi^2 V\langle|S_{21}|^2\rangle_m}{\lambda^3\eta_{1tot}\eta_{2tot}} \tag{8}$$

where V is the volume of the RC, λ is the wavelength, Q_{FD} means the Q factor measured in the frequency domain which needs to be corrected by using the total efficiency of antennas (η_{1tot} and η_{2tot}) [8]. Note that the average mode bandwidth is defined as $\Delta f = f/Q$ [16], when $\partial f = \Delta f$

$$|\langle R(\partial f)\rangle_m|_{norm,\partial f=\Delta f} = \frac{1}{\sqrt{1 + (2\pi f\tau_{RC}/Q)^2}} = \frac{1}{\sqrt{2}} \tag{9}$$

Thus a threshold of $1/\sqrt{2}$ for the autocorrelation can be used. Similar conclusions have been given in [12, 14] with different thresholds, but one should be careful on the definition of the coherence bandwidth. If $2\partial f$ is defined as the coherence bandwidth [14], a different threshold ($2/\sqrt{5}$) should be used to keep the equality between the average mode bandwidth and the coherence bandwidth, otherwise one may draw a different conclusion (i.e., the coherence bandwidth is larger than the average mode bandwidth).

Equation (7) reveals the relationship between the coherence bandwidth and τ_{RC} or Q_{TD} [14]. The use of (7) is based on the assumption that the PDP decays exponentially and the early-time response is ignored, this is reasonable as the late-time response dominates the PDP [14]. More detailed discussions on double-exponential model have been given in [14], and it has been shown that when the RC is not heavily loaded, (9) is very accurate.

B. Time Domain

The Wiener-Khinchin theorem can be used in the time domain. We can rewrite (1) in the time domain as

$$R(\partial t) \equiv \int_{-\infty}^{\infty} s(t)s^*(t + \partial t)dt = \int_{-\infty}^{\infty} s(t)s(t + \partial t)dt \tag{10}$$

where $s(t)$ is the time domain response, t is time and ∂t can be understood as the deviation for the time domain correlation. Suppose $S(f)$ is the Fourier transform (FT) of $s(t)$, (2) becomes

$$\mathcal{F}^{-1}[s(t)] = \int_{-\infty}^{\infty} s(t)e^{j2\pi ft}dt = S(-f) \quad (11)$$

because $s(t)$ is real, $S(f) = S^*(-f)$ (or $S(-f) = S^*(f)$), thus $|S(f)|^2$ is an even function, (3) becomes

$$|S(-f)|^2 = |S(f)|^2 = \mathcal{F}^{-1}[R(\partial t)] = \mathcal{F}[R(\partial t)] = \int_{-\infty}^{\infty} R(\partial t)e^{-j2\pi\partial tf}d\partial t \quad (12)$$

Interestingly, if we treat $s(t)$ as the measured time domain response of the RC, and the spectrum of the time domain response $s(t)$ is the measured S_{21}. Equation (12) reveals the relationship between Q_{FD} or chamber transfer function $\langle|S_{21}|^2\rangle_m$ and the coherence time:

$$\langle|S_{21}|^2\rangle_m = \mathcal{F}[\langle R(\partial t)\rangle_m] = \frac{Q_{FD}\lambda^3}{16\pi^2 V} \quad (13)$$

If we assume that in a narrow band $\langle|S_{21}|^2\rangle_m$ is a constant, this is reasonable as $\langle|S_{21}|^2\rangle_m$ varies slowly with the frequency. From (13), the autocorrelation $\langle R(\partial t)\rangle_m$ can be obtained as a modulated $Sa(\cdot)$ function which is

$$\langle R(\partial t)\rangle_m = \frac{2\langle|S_{21}|^2\rangle_m sin(\pi \mathrm{BW}\partial t)}{\pi\partial t}cos(2\pi f_c\partial t) = 2\langle|S_{21}|^2\rangle_m \mathrm{BW}Sa(\pi\mathrm{BW}\partial t)cos(2\pi f_c\partial t) \quad (14)$$

where BW is the frequency bandwidth of the signal, f_c is the center frequency. When $\partial t = 0$, we have

$$\langle|S_{21}|^2\rangle_m = \frac{\langle R(0)\rangle_m}{2\mathrm{BW}} \quad (15)$$

Equation (15) reveals the relationship between the autocorrelation function of the time domain response and the chamber transfer function.

C. Space Domain

When the Wiener-Khinchin theorem is applied in the space domain, the Doppler spectrum can be characterized. If the channel transfer function is changed by the rotation of a stirrer (or other moving objects), the autocorrelation function is defined as [17-20]

$$R(\partial\theta) = \int_{-\infty}^{\infty} S^*(\theta)S(\theta + \partial\theta)d\theta \quad (16)$$

where $S(\theta)$ can be the measured S_{21} at a single frequency and depends on the rotation angle θ (or position) of the stirrer, $R(\partial\theta)$ is complex-conjugate symmetric ($R(\partial\theta) = R^*(-\partial\theta)$) [17]. Following the same procedure in (2) and (3), we have

$$s(\rho) = \mathcal{F}^{-1}[S^*(\theta)] = \mathcal{F}[S(\theta)]^* \quad (17)$$

where ρ is the transformed variable of θ in FT and s is transformed from S. If θ is replaced by $\theta = vt$ where v is the rotation or moving speed and t is time in seconds, the unit of ρ is Hz.

The Doppler spectrum $D(\rho)$ is real and can be written as [17]

$$D(\rho) = |s(\rho)|^2 = \mathcal{F}^{-1}[R(\partial\theta)] = \mathcal{F}[R^*(\partial\theta)]^* = \mathcal{F}[R(-\partial\theta)]^* = \mathcal{F}[R(-\partial\theta)] \quad (18)$$

Note that the Doppler spectrum defined in (18) and the Doppler spectrum defined in [17] are symmetric in *y*-axis, but it does not affect our analysis. Also the Doppler spectrum with different moving/rotating speed v can be obtained by converting $S(\theta)$ to $S(vt)$ [17].

The relationship between the Doppler spectrum and the Q factor measured in the frequency domain can be derived. When $\partial\theta = 0$, (16) becomes

$$R(0) = \int_{-\infty}^{\infty} S(\theta)S^*(\theta)d\theta = \int_{-\infty}^{\infty}|S(\theta)|^2 d\theta \quad (19)$$

by using the Parseval's theorem (Plancherel theorem), we have

$$\int_{-\infty}^{\infty} D(\rho)d\rho = \int_{-\infty}^{\infty}|s(\rho)|^2 d\rho = \int_{-\infty}^{\infty}|S(\theta)|^2 d\theta = R(0) \quad (20)$$

Suppose $S(\theta)$ is the measured S_{21} for different stirrer angle, thus the relationship between the Doppler spectrum and Q_{FD} can be found as

$$\langle|S_{21}|^2\rangle_m = \frac{1}{\Theta}\int_0^{\Theta}|S(\theta)|^2 d\theta = \frac{1}{\Theta}\int_{-\infty}^{\infty} D(\rho)d\rho = \frac{R(0)}{\Theta} = \frac{Q_{FD}\lambda^3}{16\pi^2 V} \quad (21)$$

where Θ is the total rotation angle (or moving distance for an moving object). Comparing (21) with (15), (21) links the autocorrelation function of the frequency domain response $R(0)$ and the Doppler spectrum $D(\rho)$ to the chamber transfer function.

We can find the relationship between the *K*-factor and the Doppler spectrum. When $\rho = 0$, from (17) and (18) we have

$$|s(0)|^2 = |\mathcal{F}[S(\theta)]^*|^2_{\rho=0} = \left|\int_{-\infty}^{\infty} S(\theta)e^{-j2\pi\theta\rho}d\theta\right|^2_{\rho=0} = \Theta^2\left|\frac{1}{\Theta}\int_0^{\Theta} S(\theta)d\theta\right|^2 = \Theta^2|\langle S_{21}\rangle_m|^2 = D(0) \quad (22)$$

Note that the *K*-factor is defined as the ratio of the unstirred part and the stirred part of the received power [16, 21]

$$K = \frac{|\langle S_{21}\rangle_m|^2}{\langle|S_{21,s}|^2\rangle_m} = \frac{|\langle S_{21}\rangle_m|^2}{\langle|S_{21} - \langle S_{21}\rangle_m|^2\rangle_m} \quad (23)$$

when *K*-factor is small (the stirred part is much larger than the unstirred part $K \approx |\langle S_{21}\rangle_m|^2/\langle|S_{21}|^2\rangle_m$), by using (21) and (22), we have

$$K \approx \frac{|\langle S_{21}\rangle_m|^2}{\langle |S_{21}|^2\rangle_m} = \frac{\frac{1}{\Theta^2}D(0)}{\frac{1}{\Theta}\int_{-\infty}^{\infty} D(\rho)d\rho} = \frac{D(0)/\Theta}{\int_{-\infty}^{\infty} D(\rho)d\rho} \quad (24)$$

which gives the relationship between the *K*-factor and the Doppler spectrum. The physical meaning is clear: $D(0)$ means the DC component (zero Doppler shifts) which is the unstirred part, and the denominator represents the total power. This unifies the characterization of RC using Doppler spectrum [20] and *K*-factor [21, 22]: they are theoretically equivalent but *K*-factor gives a global description (integral) of the Doppler spectrum, while the Doppler spectrum has more detailed information.

We can also find the relationship between the *K*-factor (or the Doppler spectrum) in (24) and the total scattering cross section (TSCS) of the stirrer. By applying the Parseval's theorem to $|\langle S_{21}\rangle_m|^2$, and considering $|\langle S_{21}\rangle_m|^2$ is complex-conjugate symmetric (real), we have

$$\begin{aligned}\int_{-\infty}^{\infty}|\langle S_{21}\rangle_m|^2 df &= 2\int_{f_1}^{f_2}|\langle S_{21}\rangle_m|^2 df \\ &= \int_0^{\infty}(\mathcal{F}^{-1}\langle S_{21}\rangle_m)^2 dt \end{aligned} \quad (25)$$

If we average both sides of (25) over different antenna positions (or different stirrer positions of another stirrer), we have

$$\begin{aligned}\langle 2\int_{f_1}^{f_2}|\langle S_{21}\rangle_m|^2 df\rangle_a &= 2\int_{f_1}^{f_2}\langle|\langle S_{21}\rangle_m|^2\rangle_a df \\ &= \int_0^{\infty}\langle(\mathcal{F}^{-1}\langle S_{21}\rangle_m)^2\rangle_a dt \end{aligned} \quad (26)$$

If the early-time response from is ignored, and we check the TSCS measurement procedure in [23-26] carefully, it can be found that $\langle(\mathcal{F}^{-1}\langle S_{21}\rangle_m)^2\rangle_a$ in (26) is exactly the power decay profile of the unstirred part of the time domain response in TSCS measurement

$$\langle(\mathcal{F}^{-1}\langle S_{21}\rangle_m)^2\rangle_a \approx P_0 e^{-t/(\tau_{RC}^{-1}+\tau_s^{-1})} \quad (27)$$

where τ_s is the scattering damping time and τ_{RC} is the chamber decay time. TSCS can be obtained from [23-26] as

$$\text{TSCS} = \frac{V}{\tau_s c_0} \quad (28)$$

where V is the volume of the RC, $c_0 = 3\times10^8\ m/s$ is the speed of light in free space. If we assume $\langle|S_{21}|^2\rangle_m$ is a constant in a narrow frequency band $f_1 \sim f_2$, from (24), (26) and (27) we have

$$\begin{aligned}\langle K\rangle_{f,a} = \langle\langle K\rangle_f\rangle_a = \langle\langle K\rangle_a\rangle_f &= \frac{1}{\text{BW}}\int_{f_1}^{f_2}\langle K\rangle_a df \\ &\approx \frac{1}{\langle|S_{21}|^2\rangle_m \text{BW}}\int_{f_1}^{f_2}\langle|\langle S_{21}\rangle_m|^2\rangle_a df \\ &= \frac{1}{2\langle|S_{21}|^2\rangle_m \text{BW}}\int_0^{\infty}\langle(\mathcal{F}^{-1}\langle S_{21}\rangle_m)^2\rangle_a dt \\ &= \frac{\int_0^{\infty}P_0 e^{-t(\tau_{RC}^{-1}+\tau_s^{-1})}dt}{2\langle|S_{21}|^2\rangle_m \text{BW}} = \frac{P_0(\tau_{RC}^{-1}+\tau_s^{-1})^{-1}}{2\langle|S_{21}|^2\rangle_m \text{BW}} \end{aligned} \quad (29)$$

where $\text{BW} = f_2 - f_1$ is the frequency bandwidth. If the early-time responses of the PDP are ignored [14], similar to (25), we have

$$\begin{aligned}\int_{-\infty}^{\infty}\langle|S_{21}|^2\rangle_m df = 2\int_{f_1}^{f_2}\langle|S_{21}|^2\rangle_m df = 2\langle|S_{21}|^2\rangle_m \text{BW} \\ = \int_0^{\infty}\langle|\mathcal{F}^{-1}[S_{21}]|^2\rangle_m dt = \int_0^{\infty}P_0 e^{-t/\tau_{RC}}dt = P_0\tau_{RC} \end{aligned} \quad (30)$$

thus

$$\langle|S_{21}|^2\rangle_m = \frac{P_0\tau_{RC}}{2\text{BW}} \quad (31)$$

From (28), (29) and (31), the average *K*-factor can be obtained as

$$\langle K\rangle_{f,a} = \frac{\tau_s}{\tau_s+\tau_{RC}} = \frac{\frac{V}{\text{TSCS}c_0}}{\frac{V}{\text{TSCS}c_0}+\tau_{RC}} \quad (32)$$

where $\langle\cdot\rangle_{f,a}$ means averaging over frequencies and different antenna positions. Considering that all the loss in the RC can be equivalent to an absorber with an absorption cross section (ACS) of $\text{ACS}_{all} = V/(c_0\tau_{RC})$ [23-26], (32) can be further simplified to

$$\langle K\rangle_{f,a} = \frac{\frac{1}{\text{TSCS}}}{\frac{1}{\text{TSCS}}+\frac{1}{\text{ACS}_{all}}} = \frac{\text{ACS}_{all}}{\text{ACS}_{all}+\text{TSCS}} \quad (33)$$

which gives the relationship between the average *K*-factor and TSCS (and ACS). Note that the limit of the TSCS is a quarter of the stirring surface area $\text{TSCS} \le A_s/4$ [27], thus

$$\langle K\rangle_{f,a} \ge \frac{\text{ACS}_{all}}{\text{ACS}_{all}+A_s/4} \quad (34)$$

where A_s is the stirring surface area [27]. It is interesting to find that a lower bound for the average *K*-factor exists and it is related to the stirring surface area and the loss in the RC.

Note that when Ant 1 and Ant 2 in the RC are not high gain antennas and are not directed to each other in main lobes, the average *K*-factor obtained from frequency stir and source stir gives same results ($\langle K\rangle_{f,a} = \langle K\rangle_f = \langle K\rangle_a$), because there is no difference between averaging independent samples over different frequencies or over different antenna positions.

One can also replace the *K*-factor using the Doppler spectrum in (24) to link (33) and (34) to the Doppler spectrum, or link $\langle K\rangle_f$ to the stirrer efficiency η_s defined in [26].

III. Measurements

The measurement scenario is illustrated in Fig. 1, 1601

points of S_{21} were measured in the frequency range of 2.8 GHz ~ 3.0 GHz for each stirrer angle, 720 stirrer angles were used with a step size of 0.5°. Because the chamber decay time τ_{RC} varies slowly with frequency, a 200 MHz measurement bandwidth means that the extracted τ_{RC} is treated as a constant in the measured bandwidth, similar technique has been used in radiation efficiency measurement [8] and ACS measurement [28].

A. *Frequency Domain*

A typical set of S_{21} at one stirrer position is shown in Fig. 2, the magnitude of the autocorrelation for S_{21} in Fig. 2 is given in Fig. 3(a), and the normalized average autocorrelation over all stirrer positions is illustrated in Fig. 3(b).

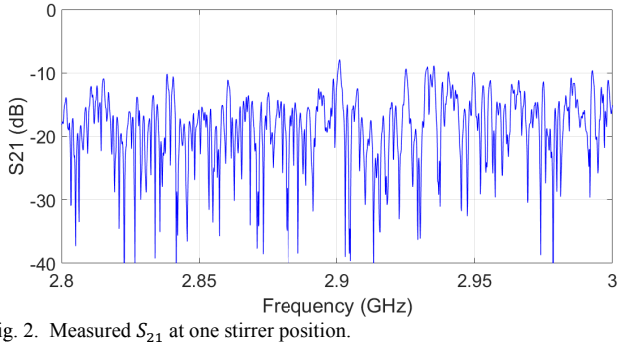

Fig. 2. Measured S_{21} at one stirrer position.

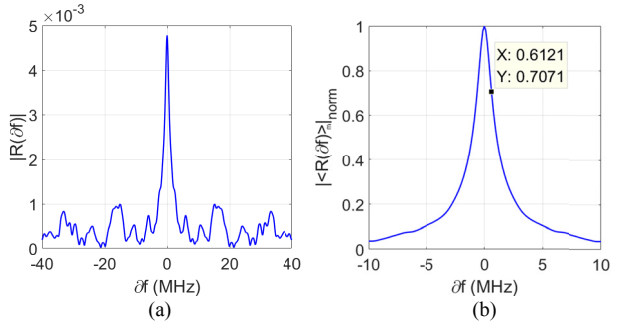

Fig. 3. (a) The magnitude of the autocorrelation for S_{21} in Fig. 2, (b) the magnitude of the normalized average autocorrelation over 720 stirrer positions.

The chamber decay time τ_{RC} can be extracted from the IFT of S_{21} measured in the frequency range of 2.8 GHz ~ 3.0 GHz [14], and is shown in Fig. 4. The least-square fitting method is used to extract τ_{RC} from PDP: the slope ratio of the fitting line is $k = -0.0163$, $\tau_{RC} = -10/(k\ln 10) = 265.79$ ns. The average mode bandwidth $\Delta f = 1/(2\pi\tau_{RC}) = 0.60$ MHz, compared with $\partial f = 0.61$ MHz at the threshold of $1/\sqrt{2} \approx 0.707$ as shown in Fig. 3(b), a good agreement is obtained. Similar measurements have been conducted in [10-14].

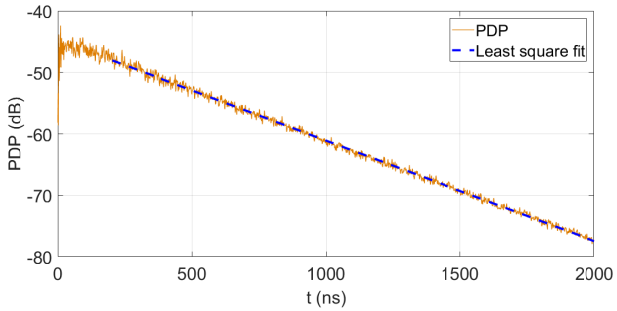

Fig. 4. PDP in dB and the least-square fit, *S*-parameters in the frequency range of 2.8 GHz – 3.0 GHz were used to obtain the time domain response.

B. *Time Domain*

The time domain response can be obtained from the IFT of the frequency domain response, it can also be measured directly by using an oscilloscope. Here we use the IFT method as a VNA normally can provide a much larger dynamic range than an oscilloscope [29].

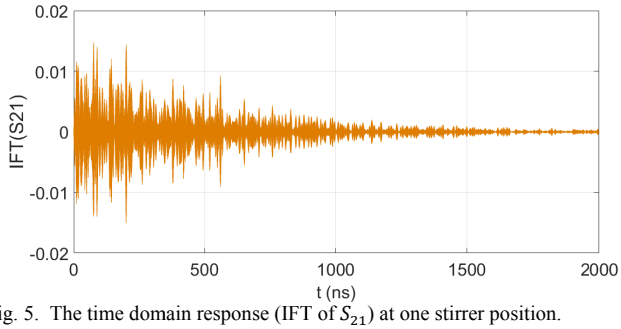

Fig. 5. The time domain response (IFT of S_{21}) at one stirrer position.

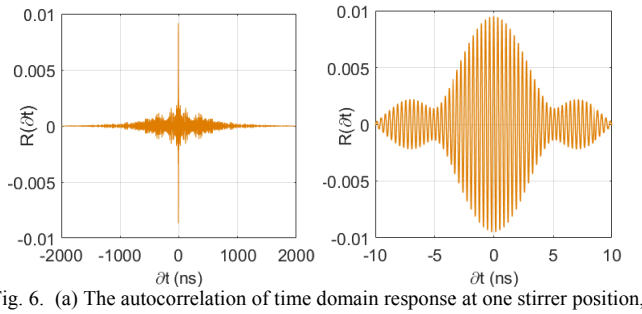

Fig. 6. (a) The autocorrelation of time domain response at one stirrer position, (b) a zoomed view.

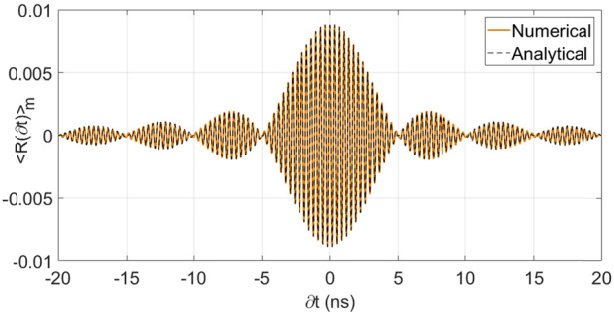

Fig. 7. The average autocorrelation over 720 stirrer positions.

A typical time domain response is illustrated in Fig. 5, the autocorrelation using (10) is calculated and plotted in Fig. 6 where Fig. 6(b) presents a zoomed view. The average autocorrelation for all stirrer positions is shown in Fig. 7, where

the analytical curve is obtained from (14) and (15) with BW = 0.2 GHz, $f_c = 2.9$ GHz, $\langle|S_{21}|^2\rangle_m = -16.5$ dB. As expected, they have a very good agreement because $\langle|S_{21}|^2\rangle_m$ is nearly constant over the frequency band. Fig. 8 gives the average transfer function obtained from the frequency domain and the FT of the time domain autocorrelation. Not surprisingly, they equal each other.

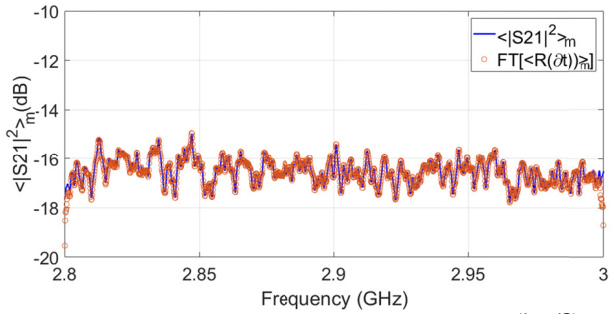

Fig. 8. The average transfer functions obtained from $\langle|S_{21}|^2\rangle_m$ and $\mathcal{F}[\langle R(\partial t)\rangle_m]$.

C. Space Domain

If we treat the measured S_{21} as a function of the rotation angle (θ) of the stirrer, at each frequency we have a set of S_{21} typically shown in Fig. 9. The magnitude and phase of the normalized average autocorrelation over 1601 frequency points are illustrated in Fig. 10. If we set the rotation speed as $1°/s$, the x-axes in Fig. 9 and Fig. 10 are in unit second, thus the unit in x-axis of the average Doppler spectrum in Fig. 11 can be Hz. The K-factor obtained from S-parameters using (23) and from Doppler spectrum using (24) are compared and given in Fig. 12. Overall they have a good agreement, but not for very small values. This is because when calculating the integral in (16), a trapezoidal numerical integration is used and has small errors.

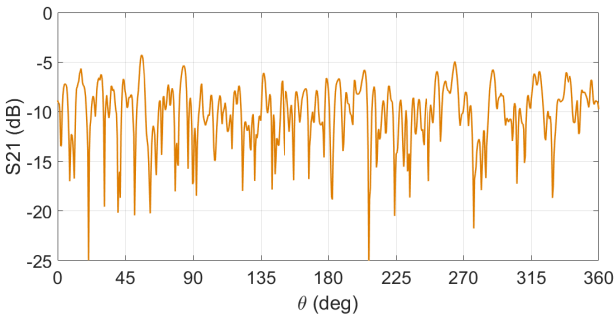

Fig. 9. Measured S_{21} at 2.8 GHz as a function of the rotation angle of the stirrer.

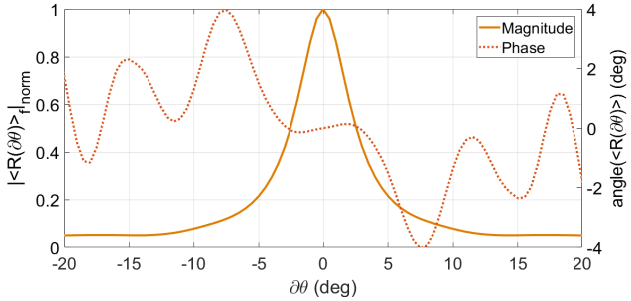

Fig. 10. The magnitude and phase of the normalized average autocorrelation over 1601 frequency points.

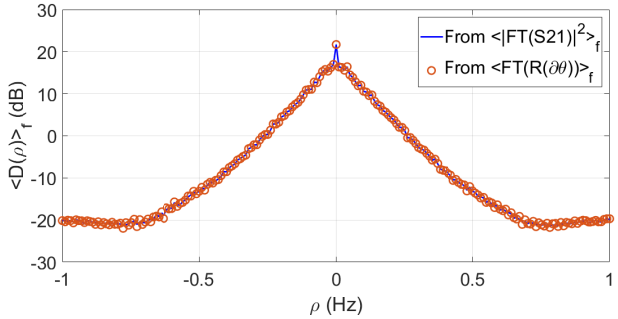

Fig. 11. Average Doppler spectrum over 1601 frequency points.

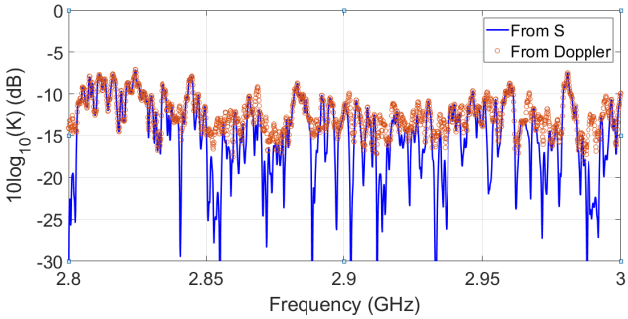

Fig. 12. Measured K-factor from S-parameters in (23) and from Doppler spectrum in (24), the lower bound of $\langle K\rangle_f$ is also given.

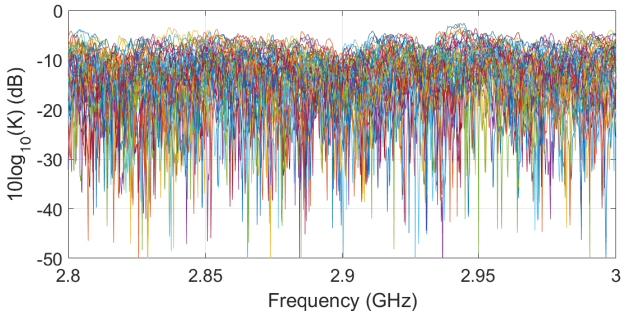

Fig. 13. Measured 50 sets of K-factors at 50 random positions of Ant 1 and Ant 2.

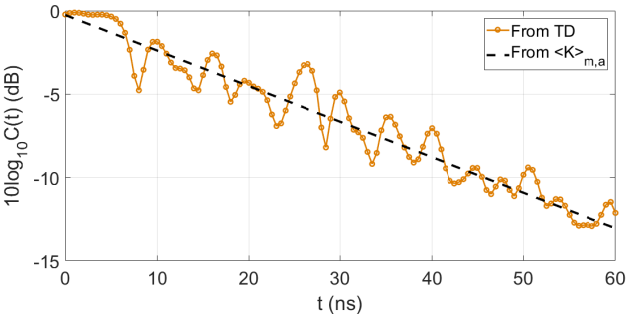

Fig. 14. A comparison of measured $C(t)$ from the time domain response and from the average K-factor.

To verify (32), we moved the positions of Ant 1 and Ant 2 in the RC with 50 positions randomly and repeated the measurement for each antenna position. Thus 50 sets of K-factors were obtained which are shown in Fig. 13, and the mean value $\langle K\rangle_{f,a} \approx -10.7$ dB. From (32), $\tau_s = \tau_{RC}/(\langle K\rangle_{f,a}^{-1} - 1)$, also note [25]

$$C(t) = \frac{\langle (\mathcal{F}^{-1}\langle S_{21}\rangle_m)^2\rangle_a}{\langle [\mathcal{F}^{-1}(S_{21})]^2\rangle_{m,a}} = e^{-t/\tau_s} \quad (35)$$

The measured $C(t)$ from time domain and e^{-t/τ_s} (τ_s calculated from $\langle K\rangle_{f,a}$) are shown in Fig. 14, which shows a good agreement. The stirring surface area of the RC is about 1.2 m^2, the lower bound of the average *K*-factor over the frequency in (34) is calculated as $\langle K\rangle_f \geq -13.4$ dB, note $\langle K\rangle_{f,a} \approx -10.7$ dB which is higher than -13.4 dB as expected.

The Doppler spectrum of other rotation speed can be derived as $D(\rho/v)/v^2$ [17], where v is the rotation speed (or moving speed), $D(\rho)$ is the Doppler spectrum for the rotation speed of $1°/s$. By replacing $\theta = vt$ in (16), Θ in (24) is the total time for one revolution of the stirrer, we have

$$\frac{D(0/v)/v^2}{\frac{\Theta}{v}\int_{-\infty}^{\infty} D(\rho/v)/v^2\, d\rho} = \frac{D(0)}{\Theta\int_{-\infty}^{\infty} D(\rho)d\rho} = \frac{|\langle S_{21}\rangle_m|^2}{\langle |S_{21}|^2\rangle_m} \approx K \quad (36)$$

As expected, the rotation speed of a stirrer does not affect the *K*-factor.

IV. Discussion and Conclusions

Different physical quantities such as coherence bandwidth/time, *K*-factor, Doppler spectrum, TSCS and ACS have been used in different applications of the RC or in RC characterizations. It would be easy to have an intuitive understanding of the relationship between these quantities, e.g. a high *Q* factor leads a small coherence time, a broader Doppler spectrum means a big stirrer, a big stirrer (TSCS) can lead to small *K*-factors and small coherence angles. However, these relationships had not been quantified and analytical equations or inequations had not been found before.

In this paper, we have shown that the Wiener-Khinchin theorem unifies different quantities in different applications: in the frequency domain, it relates the coherence bandwidth to the *Q* factor measured in the time domain; in the time domain, it relates the coherence time to the *Q* factor measured in the frequency domain; in the space domain, it relates the coherence distance/angle to the Doppler spectrum. In the meanwhile, the relationship between the average *K*-factor and the Doppler spectrum, and the relationship between the average *K*-factor and the TSCS have also been revealed. Because the TSCS has a limit [27], the lower bound of the average *K*-factor has been obtained. For large *K*-factors, the unstirred response is significant, and this effect has been quantified in [16].

The Parseval's theorem relates the *K*-factor (and the average lower bound) to the TSCS and ACS. In the derivation of the lower bound, there are two preconditions:

1. The early-time behavior of the time domain response is ignored (gated), this means that the early-time response of $\mathcal{F}^{-1}\langle S_{21}\rangle$ does not dominate the unstirred part, this is easy to satisfy when source stir $\langle\cdot\rangle_a$ is applied;
2. The unstirred part is small in (23).

Because violating these two conditions would lead a larger *K*-factor, and (34) still holds true, thus these two preconditions do not need to be satisfied and (34) is a general conclusion. However, since the average *K*-factor is not a single *K*-factor, *K*-factor smaller than the lower bound in (34) is possible for a specific antenna position in a narrow band (as can be seen in Fig. 12), but the average value over different antenna positions (or different positions for another stirrer) makes (34) valid.

It should be noted that when using (33) and (34), the average *K*-factor is related to how the TSCS is measured (how the RC is stirred). The TSCS of all the moving objects account for the average *K*-factor. By hybridizing different stirring technique, the equivalent TSCS can be increased (superimposed) [23, 26] and the lower bound can be reduced [30].

Because the TSCS can be superimposed [23, 26], (33) can be generalized to multiple stirrers:

$$\frac{1}{\langle K\rangle_{f_{all}}} - 1 \approx \sum_{i=1}^{M}\left(\frac{1}{\langle K\rangle_{fi}} - 1\right) \quad (37)$$

where $\langle K\rangle_{f_{all}}$ is the average *K*-factor when *M* stirrers moving together; $\langle K\rangle_{fi}$ is the average *K*-factor for the *i*th stirrer. The reason of using approximation (≈) is that different operation conditions of moving stirrers may not superimpose TSCS perfectly [31], although for synchronized moving stirrers the TSCS superposition has been experimentally verified [26].

References

[1] E. Genender, C. L. Holloway, K. A. Remley, J. M. Ladbury, G. Koepke and H. Garbe, "Simulating the multipath channel with a reverberation chamber: application to bit error rate measurements," *IEEE Transactions on Electromagnetic Compatibility*, vol. 52, no. 4, pp. 766-777, Nov. 2010.

[2] K. A. Remley, H. Fielitz, H. A. Shah and C. L. Holloway, "Simulating MIMO techniques in a reverberation chamber," *IEEE International Symposium on Electromagnetic Compatibility*, Long Beach, CA, USA, 2011, pp. 676-681.

[3] S. J. Floris, K. A. Remley and C. L. Holloway, "Bit error rate measurements in reverberation chambers using real-time vector receivers," *IEEE Antennas and Wireless Propagation Letters*, vol. 9, pp. 619-622, 2010.

[4] P. S. Kildal, "Overview of 6 years R&D on characterizing wireless devices in Rayleigh fading using reverberation chambers," *International workshop on Antenna Technology: Small and Smart Antennas Metamaterials and Applications*, Cambridge, UK, 2007, pp. 162-165.

[5] IEC 61000-4-21, Electromagnetic compatibility (EMC) – Part 4-21: Testing and measurement techniques – Reverberation chamber test methods, IEC Standard, Ed 2.0, 2011-01.

[6] K. A. Remley, J. Dortmans, C. Weldon, R. D. Horansky, T. B. Meurs, C. -M. Wang, D. F. Williams, C. L. Holloway and P. F. Wilson, "Configuring and verifying reverberation chambers for testing cellular wireless devices," *IEEE Transactions on Electromagnetic Compatibility*, vol. 58, no. 3, pp. 661-672, Jun. 2016.

[7] J. Yang, S. Pivnenko, T. Laitinen, J. Carlsson and X. Chen, "Measurements of diversity gain and radiation efficiency of the eleven antenna by using different measurement techniques," *4th European Conference on Antennas and Propagation (EuCAP)*, Barcelona, Spain, pp.1-5, 12-16 Apr. 2010.

[8] C. L. Holloway, H. A. Shah, R. J. Pirkl, W. F. Young, D. A. Hill and J. Ladbury, "Reverberation chamber techniques for determining the radiation and total efficiency of antennas," *IEEE Transactions on Antennas and Propagation*, vol. 60, no. 4, pp. 1758–1770, Apr. 2012.

[9] X. Chen, "Generalized statistics of antenna efficiency measurement in a reverberation chamber," *IEEE Transactions on Antennas and Propagation*, vol. 62, no. 3, pp. 1504-1507, Mar. 2014.

[10] X. Chen and P. –S. Kildal, "Theoretical derivation and measurements of the relationship between coherence bandwidth and RMS delay spread in reverberation chamber," *3rd European Conference on Antennas and Propagation*, Berlin, Germany, 2009, pp. 2687-2690.

[11] X. Chen and P. –S. Kildal, "Relations between coherence bandwidth and average mode bandwidth in reverberation chamber for wireless device measurement," *International Symposium on Antennas and Propagation (ISAP 2008)*, Taipei, Oct. 2008.

[12] X. Chen, P. S. Kildal, C. Orlenius and J. Carlsson, "Channel sounding of loaded reverberation chamber for over-the-air testing of wireless devices: coherence bandwidth versus average mode bandwidth and delay spread," *IEEE Antennas and Wireless Propagation Letters,* vol. 8, pp. 678-681, 2009.

[13] R. Armstrong, A. Marvin and J. Dawson, "An experimental investigation of the use of Q-factor to determine the shielding effectiveness of electrically large equipment enclosures with apertures," *Proc. 10th Int. Symposium on Electromagn. Compat. (EMC Europe)*, York, UK, Sep. 26-30, pp. 148-152, 2011.

[14] C. L. Holloway, H. A. Shah, R. J. Pirkl, K. A. Remley, D. A. Hill and J. Ladbury, "Early time behavior in reverberation chambers and its effect on the relationships between coherence bandwidth, chamber decay time, RMS delay spread, and the chamber buildup time," *IEEE Transactions on Electromagnetic Compatibility*, vol. 54, no. 4, pp. 714-725, Aug. 2012.

[15] E. W. Weisstein, "Wiener-Khinchin Theorem." From MathWorld--A Wolfram Web Resource. http://mathworld.wolfram.com/Wiener-KhinchinTheorem.html.

[16] D. A. Hill, Electromagnetics in Cavities: Deterministic and Statistical Theories, Wiley-IEEE, 2009.

[17] K. Karlsson, X. Chen, P. S. Kildal and J. Carlsson, "Doppler spread in reverberation chamber predicted from measurements during step-wise stationary stirring," *IEEE Antennas and Wireless Propagation Letters*, vol. 9, pp. 497-500, 2010.

[18] X. Chen, P. S. Kildal and J. Carlsson, "Determination of maximum Doppler shift in reverberation chamber using level crossing rate," *Proceedings of the 5th European Conference on Antennas and Propagation (EUCAP)*, Rome, Italy, 2011, pp. 62-65.

[19] J. H. Choi, J. H. Lee and S. O. Park, "Characterizing the impact of moving mode-stirrers on the Doppler spread spectrum in a reverberation chamber," *IEEE Antennas and Wireless Propagation Letters*, vol. 9, pp. 375-378, 2010.

[20] Z. Tian, Y. Huang and Q. Xu, "Stirring effectiveness characterization based on Doppler spread in a reverberation chamber," *10th European Conference on Antennas and Propagation (EuCAP)*, Davos, Switzerland, 2016, pp. 1-3.

[21] C. Lemoine, E. Amador and P. Besnier, "Mode-stirring efficiency of reverberation chambers based on Rician K-factor," *Electronics Letters*, vol. 47, no. 20, pp. 1114-1115, Sep. 2011.

[22] X. Chen, P. S. Kildal and S. H. Lai, "Estimation of average Rician K-Factor and average mode bandwidth in loaded reverberation chamber," *IEEE Antennas and Wireless Propagation Letters*, vol. 10, pp. 1437-1440, 2011.

[23] G. Lerosey and J. de Rosny, "Scattering cross section measurement in reverberation chamber," *IEEE Transactions on Electromagnetic Compatibility*, vol. 52, no. 2, pp. 280–284, May 2007.

[24] S. Lallechere, I. E. Baba, P. Bonnet, and F. Paladian, "Total scattering cross section improvements from electromagnetic reverberation chambers modelling and stochastic formalism," *Proc. 5th Eur. Conf. Antennas Propag. (EUCAP)*, Rome, Italy, Apr. 2011, pp. 81–85.

[25] I. E. Baba, S. Lallechere, P. Bonnet, J. Benoit, and F. Paladian, "Computing total scattering cross section from 3-D reverberation chambers time modelling," *Proc. Asia-Pac. Symp. Electromagn. Compat. (APEMC)*, Singapore, May 2012.

[26] Q. Xu, Y. Huang, L. Xing, Z. Tian, M. Stanley and S. Yuan, "B-Scan in a reverberation chamber," *IEEE Transactions on Antennas and Propagation*, vol. 64, no. 5, pp. 1740-1750, May 2016.

[27] Q. Xu, Y. Huang, L. Xing, Z. Tian, C. Song and M. Stanley, "The limit of the total scattering cross section of electrically large stirrers in a reverberation chamber," *IEEE Transactions on Electromagnetic Compatibility*, vol. 58, no. 2, pp. 623-626, Apr. 2016.

[28] Z. Tian, Y. Huang, Y. Shen and Q. Xu, "Efficient and accurate measurement of absorption cross section of a lossy object in reverberation chamber using two one-antenna methods," *IEEE Transactions on Electromagnetic Compatibility*, vol. 58, no. 3, pp. 686-693, Jun. 2016.

[29] H. G. Krauthauser, "On the measurement of total radiated power in uncalibrated reverberation chambers," *IEEE Transactions on Electromagnetic Compatibility*, vol. 49, no. 2, pp. 270-279, May 2007.

[30] X. Chen, P. S. Kildal and S. H. Lai, "Estimation of average Rician K-factor and average mode bandwidth in loaded reverberation chamber," *IEEE Antennas and Wireless Propagation Letters*, vol. 10, pp. 1437-1440, 2011.

[31] F. Moglie and V. M. Primiani, "Analysis of the independent positions of reverberation chamber stirrers as a function of their operating conditions," *IEEE Transactions on Electromagnetic Compatibility*, vol. 53, no. 2, pp. 288-295, May 2011.